Globality and Optimality in Climate Field Reconstructions from Proxy Data

M. N. EVANS, A. KAPLAN, M. A. CANE, AND R. VILLALBA

Abstract

A primary objective of paleoclimate research is the characterization of natural climate variability on time-scales of years to millennia. In this chapter, we have developed a systematic methodology for the objective and verifiable reconstruction of climate fields from sparse observational networks of proxy data, using reduced space Objective Analysis (OA). In this approach we seek to reconstruct only the leading modes of large-scale variability that are observed in the modern climate and resolved in the proxy data. Given explicit assumptions, the analysis produces climate fields and indices and their associated estimated errors. These parameters may be subsequently checked for consistency with parameter choices and procedural assumptions by comparison with withheld data and results from benchmark experiments.

The methodology is applied to the candidate tree-ring indicator data set described in Chapter 10 by Villalba et al., (2000) for the reconstruction of gridded Pacific basin sea surface temperature (SST) over the interval 1001–1990. We find that one mode of variability may be verifiably distinguished by the tree-ring indicators. This mode may be interpreted as a decadal, El Niño/Southern Oscillation (ENSO)-like pattern that influences climatic conditions in both North and South America. We speculate that this pattern is recovered because large-scale SST variability influences downstream local meteorological conditions sensed by the tree-ring data. Verification statistics for the proxy-reconstructed fields may be compared with those derived from calibrated red noise time series and from historical temperature and precipitation data collected near the proxy sampling sites. The results suggest that while credible reconstructions are possible, resolved variance is small and reconstruction errors are large, limiting interpretation to regions where there is the most skill. Additional proxy data from the Pacific coast of the Americas should improve the resolution and number of reconstructed large-scale SST modes, given that the observations are unbiased, the map describing the connection between SST and the proxy data is well defined, and appropriate observational errors have been prescribed. Copyright © 2001 by Academic Press.

Resumen

Uno de los objetivos principales de la investigación paleoclimática es la caracterización de la variabilidad climática natural en diferente escalas temporales que van desde la anual a la secular. En este estudio se ejem-

plifica el uso del Análisis Objetivo (OA) para reconstruir en forma confiable los campos climáticos globales a partir de un grupo reducido de registros paleoclimáticos. Sólo se intenta reconstruir aquellos modos dominantes de variabilidad climática de gran escala que están presentes en los datos instrumentales y que pueden ser resueltos a partir de los registros paleoclimáticos. Bajo ciertos supuestos explícitos, este análisis reconstruye campos climáticos, índices de circulación, así como los errores de estimación asociados. La consistencia de los parámetros seleccionados para las reconstrucciones bajo diferentes supuestos puede ser probado posteriormente a través de la comparación con información reservada para la verificación o con los resultados de experimentos de referencia.

En este trabajo, se aplica la metodología de OA a un grupo reducido de cronologías de anillos de árboles, descriptos en Villalba et al. (2000), con el objeto de reconstruir una grilla de temperaturas de la superficie del mar (SST) sobre el Océano Pacífico durante el intervalo 1001–1990. Se observa que uno de los modos de variabilidad en SST puede ser resuelto por el conjunto de cronologías de registros de anillos de árboles. Este modo podría ser interpretado como un modo de variabilidad decenal con un patrón espacial similar al de los eventos El Niño/Oscilación del Sur y que afecta las condiciones climáticas tanto en América del Norte como en América del Sur. El hecho de que este patrón puede ser resuelto por los registros dendrocronológicos se debe a que la variabilidad de gran escala en SST influencia las condiciones climáticas locales donde crecen los árboles muestreados. La verificación de estos campos climáticos reconstruidos a partir de los registros de anillos de árboles pueden llevarse a cabo a través de la comparación con aquellos campos derivados a partir de series temporales de ruido rojo y/o aquellos obtenidos a partir del uso de datos instrumentales de temperatura y precipitación próximos a los sitios de muestreos. Los resultados obtenidos a partir de este reducido número de cronologías sugiere que aún cuando se pueden obtener reconstrucciones confiables, el porcentaje de variancia explicado es pequeño y los errores asociados grandes, limitando la efectividad de las reconstrucciones a aquellas regiones donde los resultados son más significativos. La incorporación de un número mayor de registros paleoambientales a lo largo de la costa Pacífica de las Américas podría incrementar la resolución y el número de modos de variabilidad en SST a ser reconstruidos dado que las observaciones no son sesgadas, los mapas que describen las conecciones entre SST y los registros dendrocronológicos están bien definidos y los errores observaciones correspondientes han sido establecidos.

4.1. INTRODUCTION

4.1.1. Motivation

Much of the work in the rapidly growing field of paleoclimatology has emphasized the need to put recently observed secular climatic trends and shifts within the context of natural low-frequency variability (Martinson et al., 1995). For example, evidence for (1) global warming since the middle of the last century (Hansen and Lebedeff, 1988); (2) variations in the amplitude, duration, and frequency of El Niño/Southern Oscillation (ENSO) events (Trenberth and Shea, 1987; Trenberth and Hoar, 1996); (3) apparent state changes in the Pacific basin climate (Ebbesmeyer et al., 1991) and the timing of the Indian Monsoon (Parthasarathy et al., 1991; Krishna Kumar et al., 1999); and (4) severe mountain glacier retreat (Diaz and Graham, 1996) suggest changes in the base state of the global climate since the beginning of the Industrial Revolution. However, the processes underlying these observations are not very well understood, and some may indeed be part of quasi-periodic or low-frequency phenomena.

It has been hypothesized that many of these observations are tied to a small number of preferred, natural modes of spatial and temporal variability within the ocean–atmosphere system. Together these modes may explain much of the modern large-scale, low-frequency variance in the climate system (Wallace, 1996a,b). Examples of large-scale climatic processes are ENSO, the Pacific–North American Oscillation (PNA), and the North Atlantic Oscillation (NAO) patterns of standing atmospheric pressure waves, decadal variability in surface and intermediate circulation of the subtropical and tropical oceans (Chang et al., 1997), and globally homogeneous trends (Wallace, 1996b; Cane et al., 1997). Since these phenomena have long temporal and spatial scales, variability associated with them may be successfully retrieved from sparse observations (Miller, 1990; Cane et al., 1996). For instance, limited observations in the eastern equatorial Pacific are sufficient to crudely indicate the occurrence of an ENSO event, albeit with large uncertainties (Kaplan et al., 1998). In this chapter, we test implicitly the hypothesis that a sparse observational network composed of proxy paleoclimatic data (Epstein and Yapp, 1976; Fritts, 1976; Evans et al., 1998) may be used to reconstruct the major features of large-scale climate variability. The focus of this chapter is the development of a methodology by which we may seek skillful and verifiable reconstructions of these dominant modes using proxy data sources.

4.1.2. Proxy Climate Data and Their Interpretation

In the absence of direct physical observations, the science of paleoclimatology provides climate information through the measurement of proxies. In a broad sense these are parameters that vary in some understood way with the climatic variable of interest. Proxy measurements made on tree rings, ice cores, reef corals and sponges, sediment cores, and other geological and biological archives provide qualitative to semiquantitative estimates of climate for decades to millennia prior to the rise of direct observations (Bradley and Jones, 1992; Jones et al., 1996). Ideally, proxy observations may be used to produce what we term here a *climate field reconstruction* (CFR): a near globally complete, verifiable, and temporally continuous estimate of climate variability over some period of interest. Once we have the CFR, it is straightforward to obtain temporal indices averaged over some subarea of the global spatial domain.

The broader implications of CFR from paleoclimatic data are difficult to overestimate. Traditionally in paleoclimate research, "reconstruction" indicates recovery of a single time-varying climate index, usually of a local nature (such as seasonal air temperature from tree-ring-width chronologies) or having an immediate physical connection (such as NINO3 reconstruction from any coral site affected by ENSO). The interpretation of proxy reconstructions, usually in terms of a linear or linearized function of desired instrumental quantities, is generally verified by means of comparison with local instrumental data over a short, recent common period, although verification is increasingly made via comparison with regional or synoptic-scale observations over longer time periods. When the proxy data are contemporaneous with direct observations, opportunities are provided for intercomparison of proxy and instrumentally observed data. For example, intercomparison of independently derived proxy time series may be used to determine common features of cross-site variability. Potential biases in proxy-based records of sea surface temperature (SST) variability (age uncertainties, sampling artifacts, or other nonclimatic information) are independent of those in other proxy data or those in the bank of historical observations (instrument calibration, precision, accuracy, measurement method, frequency and spacing of sampling, and analysis procedures). In both cases, we hypothesize that common features observed across proxy realizations and in the direct observations are indicative of large-scale climatic phenomena and not small-scale or nonclimatic effects; if the instrumental and proxy data

describe climatic phenomena, then they should agree (Jones et al., 1998; Evans et al., in revision; Villalba et al., 2000; Briffa and Osborn, 1999). Such intercomparison efforts are essential for development, calibration, validation, and interpretation of individual data sets, but they may also be used to determine the potential for the development and interpretation of CFRs from proxy data (Evans et al., in revision). They provide an important link between research in climate dynamics and paleoclimatology.

Hence, we believe the most effective use of paleoclimatic data for the study of climate dynamics is via CFR based on consideration of all available proxy information, and for the reconstruction of patterns of variability, rather than point measurements. This is the idea of globality (Kaplan et al., 1997, 1998; Mann et al., 1998, 2000; Evans et al., 1998, 2000). Our view of the role of CFR as a natural link between data (proxy or instrumental) analysis and the study of climate dynamics follows the pioneering work of Fritts et al. (1971) and Fritts (1976, 1991) and is illustrated schematically in Fig. 1. Fritts provided a lucid and comprehensive introduction to the CFR concept within the context of dendroclimatological reconstruction of air temperature, sea level pressure (SLP), and precipitation anomalies over North America. More recently, the potential use of CFR on a global scale has been discussed by Jones and Briffa (1996). Bradley (1996) and Evans et al. (1998) have examined the observational array design problem, considering CFR from proxy data of varying quality and quantity. The successful extraction of variability in large-scale, low-frequency climatic phenomena from single point proxy data sources or small observational networks (Cook 1995; Wiles et al., 1998; Stahle et al., 1998; Cook et al., 2000; Evans et al., 2000; and others) has shown the potential for CFR from subsets of the available proxy paleoclimatic database. In a recent application, Mann et al. (1998, 2000) obtained very encouraging CFR results by applying space reduction and statistical techniques related to Smith et al. (1996) and Kaplan et al. (1998) for the reconstruction of surface temperature fields from several proxy data sources (Bradley and Jones 1992).

4.1.3. Globality and Optimality

The field of inverse modeling provides tools particularly suited for extraction of maximum information from a sparsely sampled, smoothly varying field. The term *Objective Analysis* (OA) encompasses a set of inverse methods employed in the estimation of the best-fit field (here in a least-squares sense) to both a sparse observational network of data and a description—a
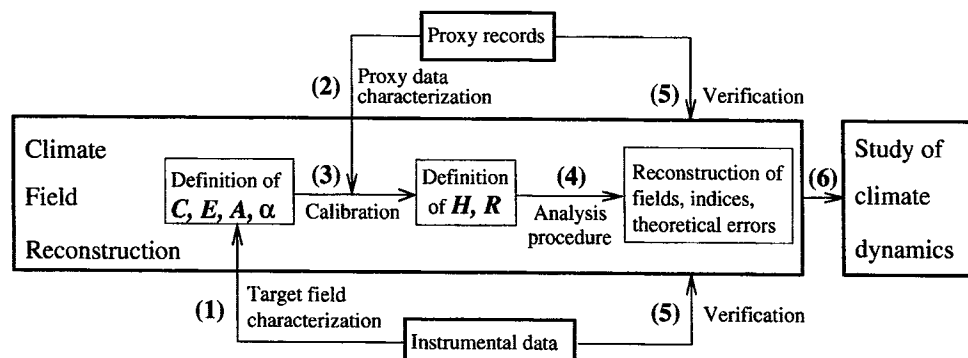
FIGURE 1 Methodology of climate field reconstruction (CFR) from proxy data. Numbered arrows on the diagram correspond to the steps in our CFR procedure (see Section 4.2).

model—of how the field varies. Errors are admitted in both the observations and the model. A cost function, consisting of the appropriately weighted squared errors in the observations and the model, is then formulated. Minimization of the cost function with respect to the field variable produces the analyzed field that is consistent with both the data and the model, given prior estimates of how precisely the model and observations are known. The error in the OA-analyzed field produced in this manner is a function of the observational error, the model error, and the extent to which the field is resolved by the observations and can be compared to either a withheld set of data for validation or to the data used in the assimilation to check the assumed observational error magnitudes.

The OA techniques have become a powerful tool used in the estimation of atmospheric and oceanographic fields of interest from spatially and temporally incomplete observations and imperfect models (Bennett, 1992; Wunsch, 1996). Special *reduced space* analogs of these techniques have been developed to reconstruct fields from sparse sampling in space and time when the fields are sufficiently smooth and have coherent, large spatial, and long temporal-scale patterns (Cane et al., 1996; Kaplan et al., 1997). Here, we apply these same tools to the reconstruction of climate fields from the even sparser but rapidly growing network of annual-resolution paleoclimate records, in order to produce CFRs from proxy data. By the reduced space rationale, we seek reconstruction of only the features of climate variability that are expected to be resolved, given the quality of the observations. Bringing the CFR problem into the context of reduced space OA provides four benefits:

1. The solution is optimal, provided the a priori assumptions hold; that is, if the data are unbiased and the covariance of a priori errors in the observations and

model are correctly estimated, then the solution obtained minimizes the squared error in the reconstructed field.

2. Space reduction emphasizes common features expressed across the proxy data set, which we expect to be climatic in origin, and discounts both climatic and proxy variability that explains little variance and is most likely to be dominated by observational errors.

3. Theoretical error estimates are provided for the solution.

4. The a priori assumptions, space reduction choices, solution, and error estimates can be tested for mutual consistency.

We illustrate this approach using the candidate data set described by Villalba et al. (2000) for the reconstruction of gridded SST for the Pacific basin over the time interval 1001–1990. The procedure is given in detail later. We focus here on the methodology of objective paleoclimatic reconstructions; the actual reconstructions shown here, which are based on a very limited number of tree-ring indicators, are not intended for interpretation. Future work will apply the methodology described here to more extensive sets of proxy indicators. Instead this methodological work is intended to complement the work of others, such as Villalba et al. (2000), who seek to characterize and interpret the climate information content of North and South American Pacific coast tree-ring chronologies. In Section 4.2, we describe the reduced space, OA CFR methodology. Section 4.3 describes the application of the technique to the reconstruction of near-global SST anomaly fields from selected Pacific-American tree-ring-width chronologies. We discuss the character of the climate information provided by tree-ring-width chronologies and conclude (Section 4.4) with some general comments on future applications of the procedure.

4.2. METHODOLOGY OF CFR FROM PROXY DATA

Our approach to CFR from proxy data will be quite similar to that applied previously to historical SST and SLP data (Kaplan et al., 1997, 1998, 2000). At all steps of the procedure we seek globality, optimality, and space reduction. The process involves six steps, which are schematically outlined in Fig. 1 and are described in detail later.

4.2.1. Characterization of the Target Climate Field

We use the modern observed data to provide estimates of the climatological mean and spatial covariance C of the target climate anomaly field. For the purpose of the study of large-scale phenomena, statistical description of the field can be further improved by first performing an optimal analysis of the historical climate data to provide reconstructions of the target climate field itself. We then determine the leading spatial modes of signal variability E (expressed as empirical orthogonal functions, or EOFs) and their energy distribution Λ (eigenvalues) through canonical decomposition of the covariance matrix C and truncation of statistically insignificant modes (Cane et al., 1996; Kaplan et al., 1997, 1998):

$$C = <TT^T> \approx E\Lambda E^T \qquad (1)$$

where boldface variables indicate vectors or matrices, $<...>$ indicates time averaging, and superscript T denotes the matrix or vector transpose. Here, E is a matrix whose columns are a relatively small number of the eigenvectors of C, and Λ is a square matrix whose diagonal elements are the eigenvalues corresponding to E. We then assume a reduced space form for the solution

$$T(t) = E\alpha(t) + residual \qquad (2)$$

where $\alpha(t)$ is the low-dimensional vector of amplitudes with which the modes E contribute to the climate field T at time t, and T is the long-term mean zero. For the modern period, the EOFs E and the vectors $\alpha(t)$ are known from the analysis of the instrumental data. For the purposes of CFR, a portion of this analyzed data set T may be used for calibration of the proxy data (see Section 4.2.3). The part of the target climate field not used for calibration purposes can then be used for independent verification of the corresponding period of the proxy-based CFR (see Section 4.2.5).

We presume the analysis of the target modern climate data captures the potential modes of variability reflected in proxy observations. Specifically, we assume that the leading patterns of pre-instrumental SST vari-ability may be adequately represented by some linear combination of the EOFs used in the analysis of the SST data. Although this assumption may be true for the largest scale patterns that are likely to be resolved by proxy data over the past several hundred years, it may be that the climate system has operated in modes that are not spanned by this characterization of the instrumental data. We also assume that the errors in this analysis are small relative to the errors in the proxy-based CFR we seek and that the climatic patterns resolved by the proxy data are a small subset of those resolved in modern historical observations.

4.2.2. Characterization of the Proxy Data

In cases where numerous proxy data realizations are expected to resolve a much smaller dimension of climatic information, we may perform a similar statistical decomposition and analysis of the proxy data, $D(t)$, to determine the leading modes of variability evident in the proxy data. In doing so, we assume that the leading modes of variability observed in the proxy data set itself are climatic in origin, rather than the expression of small-scale climatic effects or the imprint of nonclimatic influences. If this is the case, the leading eigenvalues of the decomposition may be well separated from the rest, and the corresponding EOFs will explain a large fraction of the variance in the proxy data set. This hypothesis may be checked by examining the corresponding spatial structure in the target climate field or by examining the frequency domain characteristics of the proxy amplitudes (Wallace, 1996a,b). We may also use these results to analyze the proxy data itself, following Eqs. (3)–(12) in Section 4.2.4, to emphasize common cross-site features observed in the proxy data. Such prefiltering of the proxy data reduces the potential for unrelated patterns in the proxy data to falsely project upon the leading modes of climate field variability. Statistical analyses may be checked for consistency with physical or empirical knowledge derived from development and intercomparison of the proxy data with local climatic data.

4.2.3. Calibration

We seek calibration of the proxy data $D(t)$ in terms of the time amplitudes of the reduced space representation of the climate field, $\alpha(t)$. More precisely, the low-dimensional representation of T in terms of E and $\alpha(t)$ permits the estimation scheme

$$D(t) = H\alpha(t) + \varepsilon. \qquad (3)$$

Equation (3) sets up the Gauss-Markov observational scheme for estimation of $\alpha(t)$ from the observed

proxy vector $\mathbf{D}$ (Gandin, 1965; Mardia et al., 1979; Rao, 1973). The measurement operator $\mathbf{H}$ is a linear function that maps from the climate field to the proxy observations. In other words, it represents a linear regression of the proxy data on the temporal amplitudes of the leading patterns of climate variability. For example, if $\mathbf{D}$ were SST estimates at points, then $\mathbf{H}$ would be a spatial interpolation of $\mathbf{E}$ to the observational locations. In this work $\mathbf{H}$ describes the linear function relating dimensionless tree-ring-width indices from terrestrial locales to leading modes of global SST variability. Locally, it might express the linearized relationship expected from local calibration studies or from principles of dendroclimatology.

We introduce $\mathbf{R} = <\varepsilon\varepsilon^T>$ as the matrix of observational error covariances. As defined, it is the error in observation of the climate field from the proxy data. Hence, it includes the error in observations of each proxy, the error due to space reduction [Eq. (2)], and the error in estimation of the measurement operator $\mathbf{H}$. This last error component is estimated via calibration over a limited time interval with good data coverage. Note that the construction of $\mathbf{H}$ in this manner permits nonlocal information to be recovered by the proxy data.

We use the proxy data and the instrumental data to estimate $\mathbf{H}$ and ε over a calibration interval, using the singular value decomposition (SVD). The SVD procedure decomposes the covariance between the proxy data and principal components (PCs) of the climate field into linear combinations of singular values and left and right singular vectors:

$$\mathbf{C} = <\mathbf{D}\alpha^T> = \mathbf{U}\Sigma\mathbf{V}^T \qquad (4)$$

where the columns of $\mathbf{U}$ and $\mathbf{V}$ are orthogonal vectors describing modes of covariance between the proxy data and the climate field, respectively, and $<\ldots>$ now indicates time averaging over the calibration period.

As a sparse observational network of proxy data may be expected to robustly resolve only a few leading modes of climate variability, we retain for multivariate regression with vector of coefficients $\mathbf{h}$ only the leading modes of covariance between proxy data and climate field, as defined by the SVD procedure

$$\mathbf{D} \approx \mathbf{h}\mathbf{V}_r^T\alpha. \qquad (5)$$

Here, $\mathbf{V}_r$ is the matrix consisting of the first few columns of $\mathbf{V}$. How many columns of $\mathbf{V}$ to retain is a somewhat subjective choice, though one that may be subsequently tested statistically. The use of such screening techniques to form more robust estimates of the relationships between two fields has long been applied in meteorology (Bretherton et al., 1992) and dendroclimatology (Fritts et al., 1971; Cook et al., 1994).

The vector of regression coefficients $\mathbf{h}$ is then esti-

mated based on these presumably resolvable and climatic modes:

$$\mathbf{h} = <\mathbf{D}\alpha_r^T><\alpha_r\alpha_r^T>^{-1} \qquad (6)$$

where $\alpha_r = \mathbf{V}_r^T\alpha$. The error in the map ε is the difference between the proxy observations and their best-fit estimates:

$$\varepsilon = \mathbf{D} - \mathbf{h}\alpha_r, \mathbf{R} = <\varepsilon\varepsilon^T>. \qquad (7)$$

The map from the reduced space representation of the climate field to the proxy data [cf. Eqs. (3) and (5)] is then

$$\mathbf{H} = \mathbf{h}\mathbf{V}_r^T. \qquad (8)$$

Equations (7) and (8) specify all parameters necessary for the estimation scheme given in Eq. (3).

In some cases the instrumental data and an understanding of the target climate field and its dynamics can be used to construct a model for climatic time transitions:

$$\alpha(t+1) = \mathbf{A}\alpha(t) + \varepsilon_t, \mathbf{Q} = <\varepsilon_t\varepsilon_t^T>$$

which can be used in CFR as an additional source of information for OA in an optimal smoother analysis (Kaplan et al., 1997). If no such model is available, and the signal is assumed to have zero mean, then the trivial time transition model $\mathbf{A} = 0$ may be employed:

$$\alpha(t+1) = 0\alpha(t) + \varepsilon_t, <\varepsilon_t\varepsilon_t^T> = <\alpha\alpha^T> = \Lambda.$$

This procedure assumes that the proxy measurements may be represented as a linear function of the time variability of large-scale modes of climatic variability and a residual. This functional dependence may include other factors insofar as they are linearly related to the variability exhibited by the climate field $\mathbf{T}$ within the calibration period. In fact, we have found in studies of coral $\delta^{18}O$ data that nonlocal climatic variability may constitute a significant part of the map to SST (Evans et al., 2000). We further assume that any bias in the linear relationship between climate field and proxy data is removed prior to analysis. Proxy age model uncertainty is included here only through influence on the estimated observational SST error ε in the map $\mathbf{H}$. We also assume that the map from climate field to proxy data is a robust estimate, which neither overfits nor underrepresents the climatic information in the proxy data, and that this map and its error do not change over the period of the reconstruction. These assumptions may be subsequently subjected to testing and verification (Section 4.2.5).

4.2.4. Analysis

In many observed and gridded meteorological and oceanographic fields, the number of patterns that may

be readily discerned above observational noise, data gaps, and other uncertainties is small. For CFR based on proxy data, the number of observations is much smaller and the observational error is far larger, so the dimension of the resolvable climatic *space* is expected to be even smaller.

We seek the field $T(x,t)$, which is the best fit to the proxy observations constrained to be near the spatial target field covariance. We construct a cost function

$$S(\alpha) = (D - H\alpha)^T R^{-1}(D - H\alpha) + \alpha^T \Lambda^{-1}\alpha \qquad (9)$$

S evaluated at each time t is a unitless scalar quantity. Here, α is the vector of temporal amplitudes we seek to reconstruct from the proxy data. The first term of Eq. (9) represents the squared residuals between the proxy observations and their α-based predictions at each time t. R is the estimate of their covariance [Eq. (7)] and weights this set of residuals. Similarly, the second term weights the *residuals* of the trivial prediction model $\alpha = 0$ with its inverted error covariance, which is the covariance of the signal [Eq. (1)]. At each time t, the analysis is punished ($S \rightarrow$ large) for putting too much stock either in observations with large error or in patterns that explain little of the energy in the spatial covariance patterns observed in the modern SST field (Kaplan et al., 1997).

Minimization of a quadratic cost function such as Eq. (9) retrieves the generalized least-squares estimate of α (Sokal and Rohlf, 1995). If the proxy observations are unbiased, and if the a priori error covariances R and Λ are well estimated and uncorrelated in time, then minimization of S produces the best linear unbiased estimate (BLUE) (Mardia et al., 1979). For this specific minimization problem, in which S has been written in terms of reduced space variables, minimization at each time t produces the reduced space optimal estimate (Kaplan et al., 1997):

$$\alpha(t) = PH^T R^{-1} D(t) \qquad (10)$$

and the field T is recovered by Eq. (2)

$$T(t) = E\alpha(t). \qquad (11)$$

P is the error covariance in the estimate T:

$$P = (H^T R^{-1} H + \Lambda^{-1})^{-1} \qquad (12)$$

and it represents a weighted average of the error in the observations mapped to the analysis domain and the spatial field covariance estimate. The weights are determined by the observational error covariance matrix R, and the variance Λ is resolved by the EOFs E over the calibration period. The rank of H is determined as part of the calibration procedure (Section 4.3.3). The matrix H in Eqs. (10) and (12) consists of the rows of H defined by Eq. (8) for which the proxy data are avail-

able at analysis time t. When the observations are relatively accurate (R small) or sufficiently numerous (H has high row dimension), the analysis error is low, and the analysis puts variance into the solution T. When observations are poor (R large) or absent (H has low row dimension), the analysis error is large, and the analysis estimate T approaches climatology (e.g., the trivial solution $T = 0$). Similarly, if the proxy data do not skillfully describe climatic variance over the calibration period (H of low rank and/or R large), the analysis estimate T will have low amplitude. In either case, the analysis error covariance is formulated to be consistent with our a priori assumptions about the error in the observations, map, and model; our error covariance estimates; and the availability of proxy observations over time. Subsequent verification exercises may show that we have assumed the proxy data are too accurate or the relationship between proxy data and climate field is too well resolved. Iteration of the procedure, with different choices for the rank of H and more reasonable estimates of R, is required until a priori assumptions match a posteriori results and produce the optimal analysis field estimate T.

4.2.5. Verification

The initial verification of the reconstructed climate field is a comparison with the observed climate data withheld from the calibration procedure (Sections 4.2.1 and 4.3.3). The more complicated issue is testing the consistency of the analysis, as was mentioned earlier. Technically, the analysis solution is optimal, provided the proxy calibration holds for the entire period of reconstruction; the data and model are unbiased estimates; and the observational error ϵ is uncorrelated in time. We may test the validity of these assumptions via cross-validation experiments with withheld data, comparison of the verification residuals with the theoretical error in the analysis, and comparison of the analysis results with other independent data (instrumental or proxy). In addition, to determine the extent to which climatic information is resolved by the proxy data, the proxy-based CFR may be compared to CFRs based on synthetic proxy data chosen to represent benchmark observations or data sets devoid of information.

4.2.6. Study of Climate Dynamics

Once the reconstruction field T has been satisfactorily validated, we may begin to study it as a source of climatic information within the context of its strengths and limitations. In many cases, the analysis error will be quite large and will limit interpretation to only the largest scale area-average indices. Such indices may be

subjected to time series analysis, epoch analysis, frequency domain analysis, joint spatial-temporal mode analysis, and climate change hypothesis testing. Many such studies become more direct and convenient when the reduced space form of the solution [Eqs. (10) and (12)] is utilized.

4.3. APPLICATION: PACIFIC BASIN SST FIELD RECONSTRUCTION FROM PACIFIC AMERICAN TREE-RING INDICATORS

4.3.1. Target Climate Field

SST is an important diagnostic of the global climate. The surface ocean and atmosphere participate (or are suspected to participate) in positive and negative dynamical feedback mechanisms on a wide range of timescales (Namias, 1969, 1980; Cane, 1986; Deser et al., 1996; Latif and Barnett, 1994; Lau and Nath, 1994; Webster, 1994; Trenberth and Hurrell, 1994; Clement et al., 1996; Cane et al., 1997; Clement, 1998). As a statistical field, SST varies relatively smoothly on large time and space scales, and so we hypothesize that its leading temporal and spatial covariance patterns are likely to be captured by a sparse observational network composed of proxy observations.

Our source of SST data for use as a target climate field is the recently produced analysis (Kaplan et al., 1998) of the MOHSST5 (Parker et al., 1994) product of the U.K. Meteorological Office. MOHSST5 is a 5° × 5° monthly compilation of historical (1856–1991) ship-based observations of SST, and the Kaplan et al., (1998) analysis employs the newly developed technique of the reduced space optimal smoother to objectively extract large-scale variations of SST from incomplete spatial and temporal observational coverage. Variance on small spatial scales, amounting to $(0.3–0.4)^2$ °C^2 of the intermonthly variance, which is not constrained by the observations, is filtered out by the reduction of the EOF space. The analysis can reconstruct anomalies associated with ENSO and other large-scale phenomena, including low-frequency variability (Enfield and Mestas-Nuñez, 2000; for several examples and tests, see Kaplan et al., 1998). Since our purpose is the reconstruction of large-scale SST field variability, we chose this product as our basis or *target* climate field for our CFR experiment.

We use 1856–1990 annual means of Pacific basin SST anomaly (87.5°N to 87.5°S, 110°E to 65°W) from this analysis (hereafter termed KaSSTa) as our target climate field. The annual average runs from April of the current year through March of the following year, the natural year for much of the Pacific Ocean (Ropelew-

ski and Halpert, 1987). This choice also serves to integrate dendroclimatological anomalies observed in the Northern Hemisphere growing season (April–October) and those observed during the growing season of the Southern Hemisphere (November–March), which together provide complementary information on annually averaged SST anomaly (Villalba et al., 2000). Following Kaplan et al., (1998), these data are decomposed into a set of EOF weights and temporal loadings, and the leading 30 modes of spatial variability are used to reconstruct approximately 85% of the total variance in the annually averaged gridded 5° × 5° estimates of SST anomaly on which KaSSTa is based (Bottomley et al., 1990). The domain, variance, and error in the analysis of this target climate field are shown in Fig. 2.

4.3.2. Proxy Data

For over a century, those in the field of dendroclimatology have sought estimates of local and regional climate variability from measurements made on trees producing marked annual growth rings (Fritts, 1976, 1991). One of the most common measurements is the width of sequential annual rings. In an individual tree, rings indicate the passage of time, and ring-width variations reflect the combined effects of biophysical and environmental factors, including climate. While the physiological factors controlling ring-width variations within individual trees are complex and difficult to quantify (Fritts et al., 1971), the mean weather and climatic conditions at a given site should have a similar effect on all trees within a homogeneous stand. In addition, using a priori knowledge of local or regional growing conditions, the sampling site may be chosen for its expected sensitivity to a particular, growth-limiting climatic variable of interest (Fritts, 1976). Dendroclimatologists employ statistical approaches to determine the common climatic signal extricable from a population of trees; such a statistical reduction of the data to a well-dated, continuous, standardized, tree-growth index is known as standardization, and its final product is called a chronology.

Many hundreds of tree-ring-width chronologies have now been developed worldwide (ITRDB, 1998), and their relationships to climatic variables have been tested on local, regional, and global scales. In a recent application, Villalba et al. (2000) found that tree-ring-based estimates of air temperature and drought developed from Pacific American tree-ring chronologies share a common, decadal mode of time variability over the last four centuries. They showed that this variability is associated with an ENSO-like pattern of SST anomalies in the Pacific basin. With the hypothesis that this SST pattern forces variability observed in the proxy
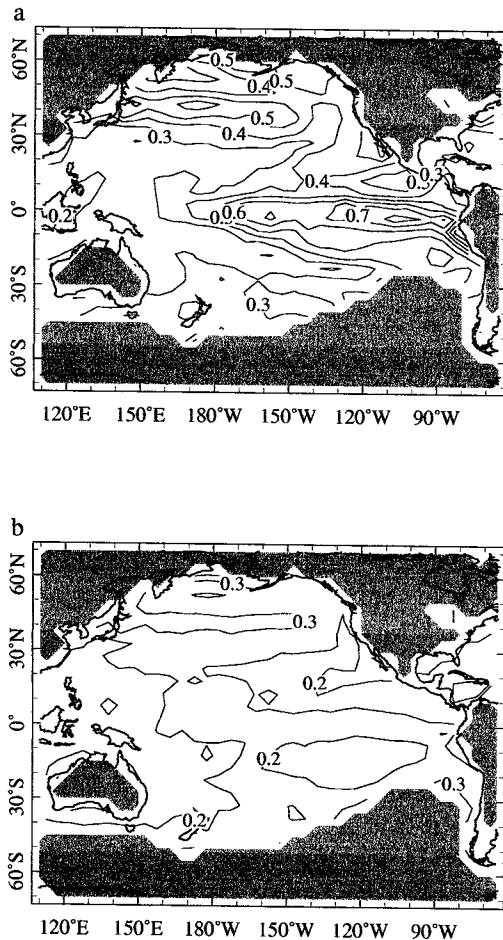
FIGURE 2 (a) The target climate field of the annually averaged Pacific basin sea surface temperature (SST) anomaly. Contours give root-mean-squared (RMS) variance in degrees Celsius (°C). (b) Error in estimation of the field (°C). Gray areas show regions where there are insufficient data for analysis. (Data from Kaplan et al., 1998.)

data, they inferred increased energy associated with the decadal SST pattern during the period 1600–1850, relative to the present (Villalba et al., 2000).

Following the intriguing and encouraging results of Villalba et al. (2000), we hypothesize that large-scale SST anomalies over the Pacific basin give rise to surface air temperature, precipitation, and drought anomalies across the tropical and extratropical Americas; in turn, dendroclimatological data from affected regions may be used to reconstruct the relevant SST variability. Hence, we apply the approach detailed earlier in Section 4.2 to the problem of reconstructing Pacific basin SSTs from the small subset of dendroclimatological indicators studied by Villalba et al. (2000) (Table 1) for the interval 1001–1990. For our purposes, we term these data *tree-ring indicators* of climate variability, noting that the data have a diversity of sensitivities (lo-

cal air temperature, precipitation, or both, in the case of drought indicators) and include tree-ring-width chronologies as well as climatic indices derived from tree-ring-width chronologies.

To compare and evaluate the results, we apply the same methodology to reconstruct SST from two additional sets of indicators. The first is a set composed of instrumental climate data from the locations from which the proxy data were collected (Table 1). These are selected to mimic the expected sensitivity (to surface temperature, precipitation, and drought) of the dendroclimatological data employed. The second is a set of red noise processes with lag –1 autoregressive characteristics like those of the dendroclimatological data. These two additional benchmark and noise reconstruction experiments are expected to return estimates of the best possible reconstruction results and of skill expected by chance, respectively. In all cases, the proxy indicators have been normalized, as their original variances relative to one another may or may not have climatic significance.

4.3.3. Calibration

4.3.3.1. Construction of the Relationship between SST and Tree-Ring Indicators

Finding the appropriate mapping **H** from the SST to the proxy data is a somewhat subjective task that we solve in the following manner: we estimate the covariance matrix between the proxy data and the low-dimensional vector of amplitudes known from KaSSTa over the calibration interval 1923–90 [Eqs. (3) to (8)] and we reserve the complementary part of the KaSSTa amplitudes (1856–1922) for verification exercises and as an alternate calibration period (see Section 4.3.5. Following the work of many dendroclimatological calibration studies in general (Fritts, 1976) and employing the findings of Villalba et al. (2000) in particular, we permit the tree-ring data to provide information on SST variability through simultaneous and lag –1 year covariances.

EOF analysis of the tree-ring data suggests that this data set has at least one and perhaps up to three significant EOFs. The first proxy EOF, which explains about 32% of the variance in the time series, is clearly distinguishable above the eigenvalue spectrum retrieved from EOF analysis of red noise time series with the autoregressive characteristics of the tree-ring data (Fig. 3). Similar decomposition of the observed data suggests that, at most, two to three significant EOFs may be retrieved from the sampled regions.

Considering these results and the work of Villalba et al. (2000), we present the analysis with only the leading

TABLE 1   Tree-Ring Indicators Used in This Analysis[a,b]

Site name	Latitude	Longitude	Interval	Benchmark historical time series
Coast of Alaska—temperature sensitive (Wiles et al., 1998)				
Ellsworth	60.2°N	149.0°W	1580–1991	
Exit Glacier	60.2°N	149.6°W	1580–1988	
Miners Wells	60.0°N	141.7°W	1580–1995	
Tebenkof	60.8°N	148.5°W	1580–1991	SST at (57.5°N, 142.5°W)
Verstovia Ridge	57.0°N	135.3°W	1580–1996	
Whittier	60.8°N	148.6°W	1580–1991	
Wolverine Glacier	60.3°N	148.9°W	1580–1991	
Northern Patagonia—temperature sensitive (Villalba et al., 1997)				
Castaño Overo	41.2°S	71.8°W	1540–1991	
Castaño Overo	41.2°S	71.8°W	1550–1991	SST (42.5°S, 72.5°W)
Co. D. de León	41.3°S	71.7°W	1564–1991	
Southwestern U.S.—drought sensitive (Cook et al., 1999)				
TrPDSI Cell 53	31.0°N	107.5°W	1693–1978	PDSI (31.0°N, 107.5°W)
TrPDSI Cell 63	31.0°N	104.5°W	1690–1978	PDSI (31.0°N, 104.5°W)
TrPDSI Cell 80	39.0°N	98.5°W	1680–1978	PDSI (39.0°N, 98.5°W)
TrPDSI Cell 81	37.0°N	98.5°W	1698–1979	PDSI (37.0°N, 98.5°W)
Northern Patagonia—precipitation sensitive (LaMarche et al., 1979)				
El Asiento	32.7°N	70.8°W	1001–1996	Santiago, Chile, precipitation (33.5°S, 71.5°W)

[a]For more information on the selection of these proxy indicators, see Villalba et al. (2000).

[b]TrPDSI is the gridded estimate of the Palmer Drought Severity Index (PDSI) reconstructed from tree-ring chronologies (Cook et al., 1999).

singular vector of the covariance between SST and proxy data retained. (We leave as a verification exercise [Section 4.3.5] determination of whether additional singular vectors add appreciably to the skill of the reconstruction.) Figure 4 shows the spatial pattern associated with the time series of the leading singular vector for
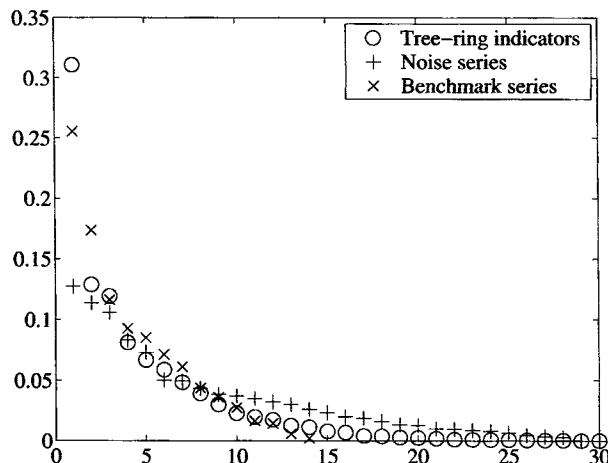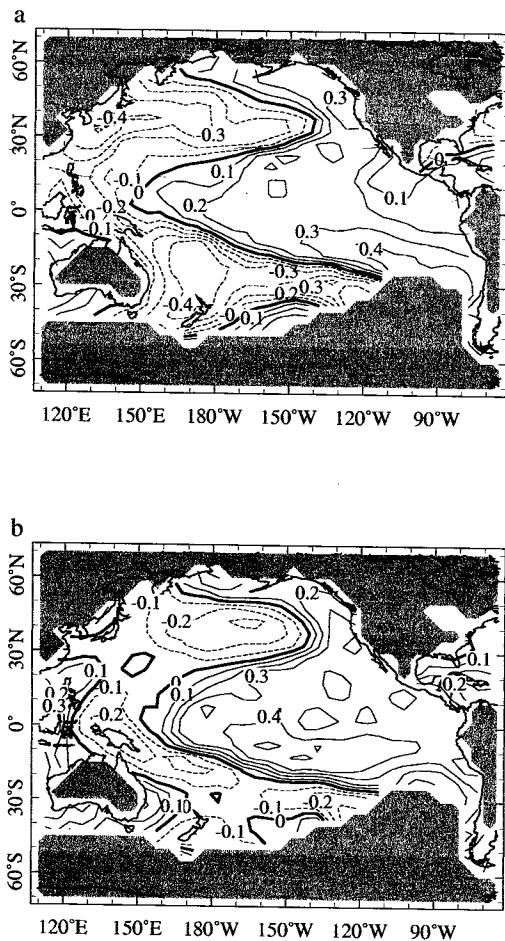
both the proxy data and benchmark data calibration experiments. Not surprisingly, the proxy calibration captures the same pattern Villalba et al. (2000) observed. Resolution of this pattern is corroborated by a similar (but stronger) pattern from analysis of the benchmark instrumental data set (Table 1). However, the error in the resolution of this pattern [$\mathbf{R}$, Eq. (7)] is large in both cases, due to the difficulty with which these sparse observational networks discern the climatic variability. Results described later show that observational error variances are, on average, about 80% of the signal variance.

4.3.3.2. Contribution of Individual Indicators to the Reconstructed Mode

Table 2 shows the correlations of individual tree-ring indicators with the single mode of reconstructed SST variability as a function of calibration period and time lag. We interpret these correlations as the contribution made by each indicator to the reconstructed pattern. Lag 0 or lag +1 correlations that are significant above the 90% confidence level in both calibration periods are in bold. Seven of the indicators (3, 4, 5, 7, 9, 12, and 15) meet these criteria for simultaneous correlations, and nine (2, 3, 4, 5, 7, 9, 11, 12, and 14) meet these criteria for lag +1 correlations. Six indicators (3, 4, 5, 7, 9, and

FIGURE 3   Eigenvalue spectrum of the tree-ring data employed in this study (O). For reference, the eigenvalues of red noise time series with similar autocovariance statistics (+) and of historical observations from the proxy sampling sites (×) are also shown.

FIGURE 4 (a) Correlation of the first tree-ring principal component (PC) with the sea surface temperature (SST) field. (b) Correlation of the first PC derived from benchmark instrumental observations with the SST field.

TABLE 2 Contribution of Tree-Ring Indicators to Reconstruction

Correlation with time series of reconstructed pattern[a]

	1923–1990 calibration		1856–1922 calibration	
Indicator[b]	Lag 0	Lag +1	Lag 0	Lag +1
1 CAT	0.42 (99)	0.45 (99)	−0.17 (14)	0.06 (64)
2 CAT	0.18 (86)	**0.24** (93)	0.14 (82)	**0.30** (97)
3 CAT	**0.54** (99)	**0.58** (99)	**0.53** (99)	**0.72** (99)
4 CAT	**0.31** (97)	**0.25** (93)	**0.24** (93)	**0.33** (98)
5 CAT	**0.52** (99)	**0.45** (99)	**0.37** (99)	**0.64** (99)
6 CAT	0.31 (96)	0.26 (94)	−0.01 (50)	0.11 (75)
7 CAT	**0.42** (99)	**0.49** (99)	**0.22** (93)	**0.37** (99)
8 NPT	0.37 (99)	0.33 (98)	0.11 (73)	0.17 (86)
9 NPT	**0.51** (99)	**0.31** (98)	**0.21** (91)	**0.21** (92)
10 NPT	0.37 (99)	0.36 (98)	0.13 (83)	0.15 (86)
11 SWP	0.02 (56)	**0.71** (99)	0.28 (98)	**0.71** (99)
12 SWP	**0.20** (94)	**0.76** (99)	**0.47** (99)	**0.71** (99)
13 SWP	−0.24 (92)	0.14 (80)	0.17 (86)	0.54 (99)
14 SWP	−0.18 (88)	**0.29** (97)	0.22 (92)	**0.64** (99)
15 NPP	**0.25** (94)	0.35 (99)	**0.39** (99)	0.05 (63)

[a]Numbers in parentheses give percent confidence level estimates, which are based on correlations with 1000 synthetic time series having first-order autoregressive characteristics of the tree-ring indicators. Lag 0 or lag +1 correlations significant above the 90% level in both calibration periods are in bold.

[b]Sensitivity of indicator to local conditions as described by Villalba et al. (2000): CAT, coastal Alaskan temperature; NPT, northern Patagonian temperature; SWP, southwest U.S. Palmer Drought Severity Index (PDSI); and NPP, northern Patagonian precipitation.

12) are significantly correlated with the reconstructed mode at both lags and in both calibration periods. These subsets of indicators include precipitation- and temperature-sensitive tree-ring indicators from both hemispheres, in agreement with the hypothesis (Villalba et al., 2000) that the resolved SST pattern represents a common forcing of both Northern and Southern Hemisphere extratropical temperature and precipitation anomalies. Consequently, the reconstructed SST pattern produced independently by using the 1923–90 and 1856–1922 calibration intervals share almost 60% variance. However, the results also show that several indicators (1, 6, 8, and 13) did not contribute consistently within both calibration periods or for either lag relationship to the reconstruction, and two (13 and 14) changed the sign of their simultaneous correlations between calibration periods.

If the assumption is made that the relationships between SST and tree-ring-site climate represented statis-

tically here have not shifted in space, and if the targeted single mode of SST continues to be the desired reconstruction target, then these results may suggest that an additional level of data screening is necessary. For example, Villalba et al. (2000) make this assumption to argue that the tree-ring data indicate different temporal variability before and after 1850. Ten of the fifteen tree-ring indicators support this assumption for the 1856–1990 period by calibrating in the same manner over both halves of the full period (Table 2). However, several indicators (1, 6, 8, 10, and 13) were significantly correlated during one calibration period, but not within the other. This result suggests that either a real change in the relationship between tree-ring indicator and SST or that the observed relationship is weak. We cannot eliminate the influence of real changes in either the proxy SST relationship or the proxy local climate relationship on long timescales. Further steps to test the stationarity assumption may include data-screening experiments with the current proxy data set, incorporation of additional tree-ring indicators from locations sensing the identified mode of climate variability, and quantitative estimation of the sensitivity of tree-ring in-
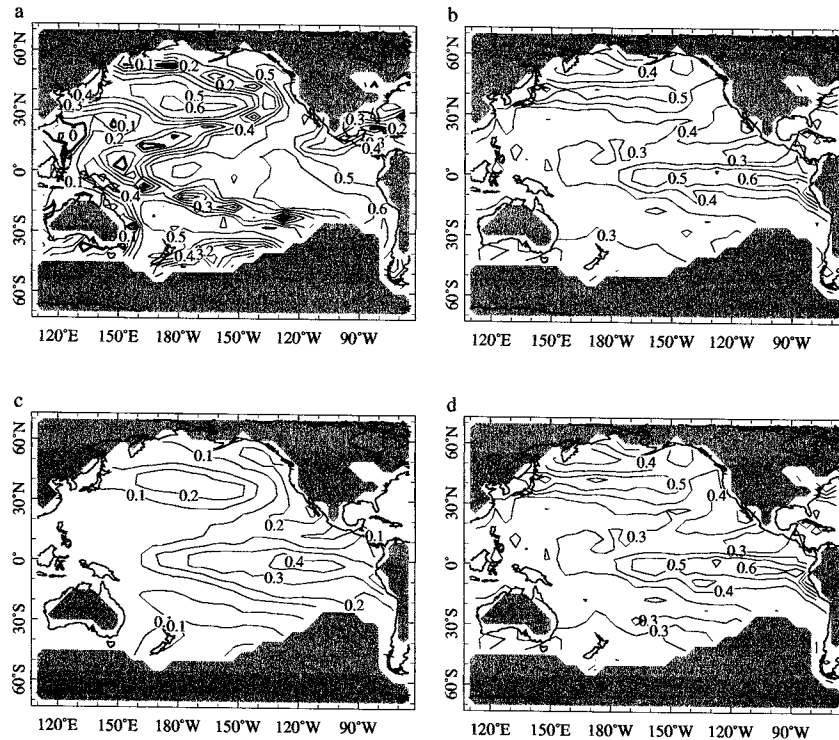
FIGURE 5 Calibration statistics for reconstruction using the 1923–90 calibration interval. All statistics are calculated by using 1923–90 data from Kaplan et al. (1998) (here termed KaSSTa) and the tree-ring-based SST reconstruction (TrSSTa) results. (a) Field correlation (correlation units). (b) Root-mean-squared (RMS) difference between TrSSTa and KaSSTa (°C). (c) RMS variance in TrSSTa (°C). (d) Theoretical error for TrSSTa (°C).

dicators to local climate variables. Analysis of the physical differences between these sites and nearby sites with significant contributions to the reconstruction may indicate reasons for calibration failures and may suggest additional locations from which proxy data may be usefully incorporated or collected. These steps may all serve to reduce or better estimate the observational and mapping error in the reconstruction procedure through better understanding of the physical and biological processes underlying the statistical relationships observed here.

4.3.4. Analysis

We first examine results using 1923–90 as a calibration period, reserving data for 1856–1922 for verification exercises. Four statistics calculated for each point in the analysis grid are shown in Figs. 5 and 6 for calibration and verification periods, respectively. Correlation between reconstructed (TrSSTa) and verification (KaSSTa) fields shows where the reconstruction has skill regardless of signal amplitude (panel a). The root-mean-squared (RMS) difference between TrSSTa and

KaSSTa gives the actual error in the reconstructed fields by comparison of withheld observed data and reconstruction results (panel b). Panel (c) shows the RMS variance in the reconstructed field; this map may be compared to Fig. 2 to assess the extent to which the analysis resolves variance. Panel (d) gives the theoretical error in TrSSTa averaged over the verification period. This map may be compared to the RMS difference described previously to determine consistency of the reconstruction's theoretical error estimate.

4.3.5. Verification

4.3.5.1. Consistency of A Priori Assumptions and A Posteriori Results

Calibration results (Fig. 5) for the 1923–90 period show that correlation between TrSSTa and KaSSTa reaches 0.4–0.6 over much of the eastern tropical Pacific and in the centers of the Pacific subtropical gyres. This result indicates that ca. 20–25% of the variance in KaSSTa was calibrated in these regions, consistent with the map of reconstructed RMS variance in TrSSTa (Fig.
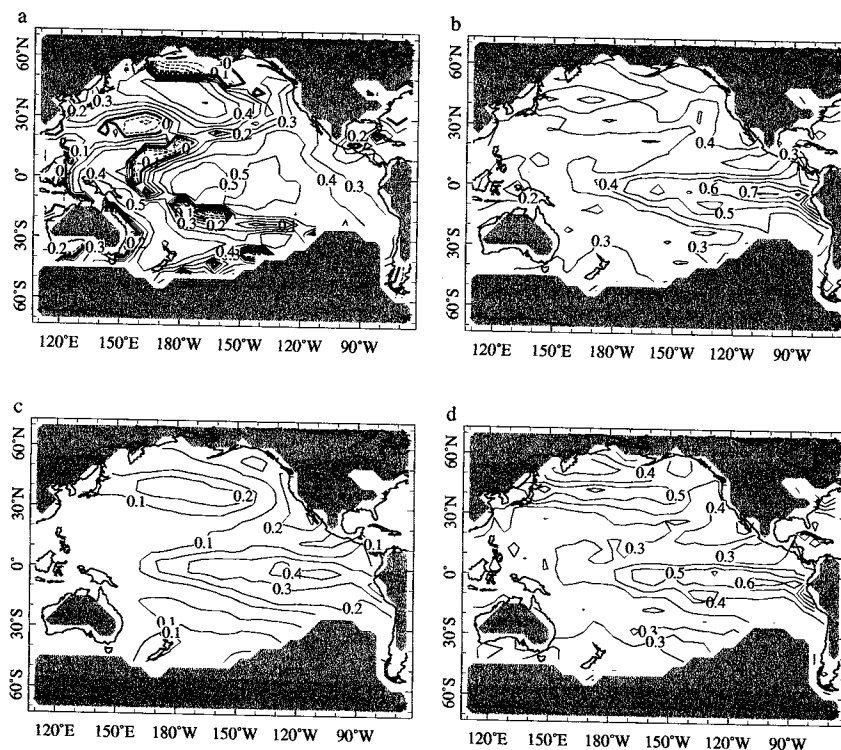
FIGURE 6 Verification statistics for reconstruction using the 1923–90 calibration interval. All statistics are calculated by using 1856–1922 data from Kaplan et al. (1998) (here termed KaSSTa) and the tree-ring-based SST reconstruction (TrSSTa) results. (a) Field correlation (correlation units). (b) Root-mean-squared (RMS) difference (°C). (c) RMS variance in TrSSTa (°C). (d) Theoretical error for TrSSTa (°C).

5c), which has roughly one-fourth to one-fifth of the amplitude of KaSSTa (Fig. 2a) over this period. Areas of minimum correlation correspond to regions in which the map **H** has little amplitude. Retrieval of small-amplitude TrSSTa is consistent with the large error in resolution of **H** shown in Fig. 4; the error plots (Figs. 5b and 5d) indicate that the mapped variance in the eastern equatorial Pacific and in the subtropical gyres is only partially resolved. Comparison of the actual RMS error and average theoretical error estimates (Figs. 5b and 5d) shows that the analysis procedure produces self-consistent errors.

4.3.5.2. Comparison with Withheld Historical SST Data

Results (Fig. 6) computed over the 1856–1922 verification period are similar to those shown in Fig. 5, suggesting that TrSSTa has captured limited but verifiable climatic information. Correlations have shrunk in amplitude by 0.1–0.2 units in the regions in which **H** has nonzero amplitude, but are similar in spatial pattern and strength to the results shown for the calibration period. This result suggests that the resolved pattern is ro-

bustly defined, at least for the interval 1856–1990, and serves as an initial check of analysis assumptions. An overlay of the correlation map shown in Fig. 4 with the verification correlation of TrSSTa and KaSSTa clearly shows that regions with the best reconstruction skill are also regions where the resolved map has a large amplitude; regions of minimal reconstruction skill correspond to regions of minimal map amplitude (Fig. 7 [see color insert]). Actual and theoretical error estimates are approximately equal (Figs. 6b and 6d), suggesting that we have not overcalibrated the reconstruction by retaining modes that cannot be verifiably reconstructed. However, note that the error in the North Pacific region has a slightly different structure than the actual error.

4.3.5.3. Sensitivity to the Calibration Period

We exchange the calibration and verification periods chosen for the previous experiment to estimate the dependence of the map from SST to tree-ring indicators on the calibration interval. The same four statistics are plotted for a 1856–1922 calibration period and a 1923–90 verification period in Figs. 8 and 9, respectively. Calibration results (Fig. 8) give slightly improved skill, but
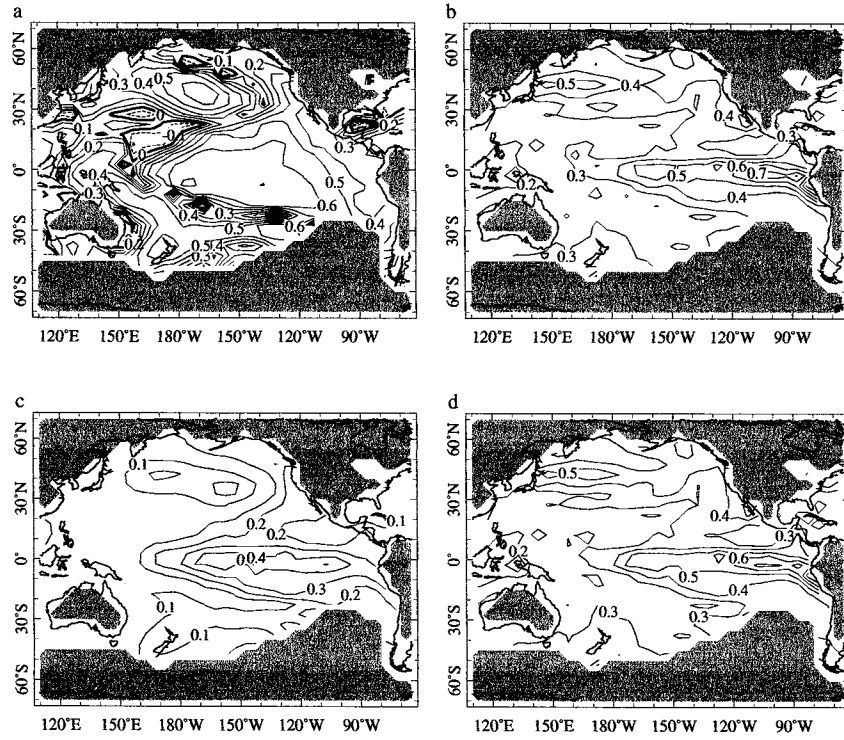
FIGURE 8 Calibration statistics for reconstruction using the 1856–1922 calibration interval (as in Fig. 5).
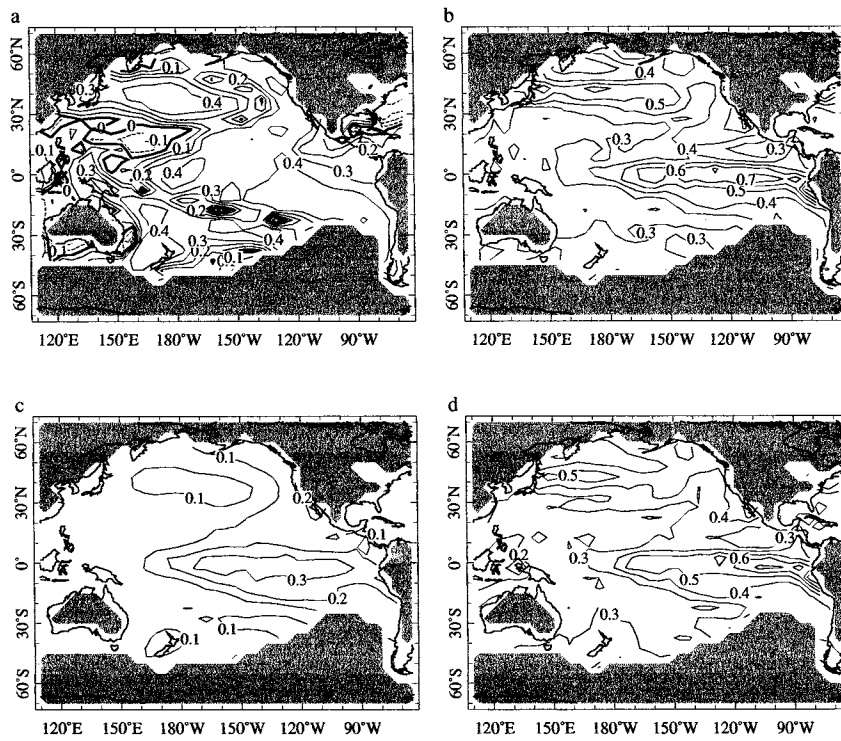
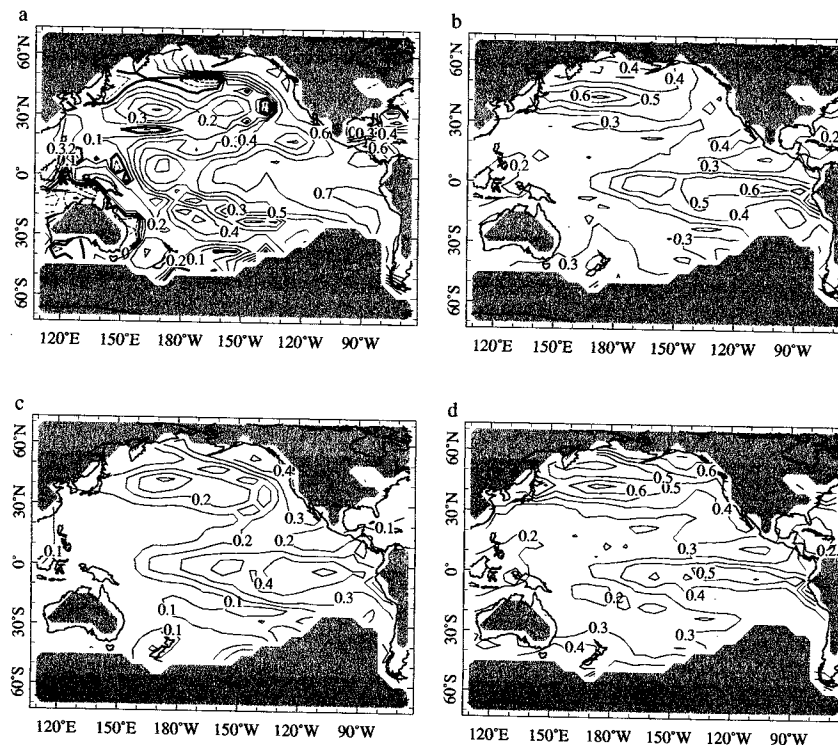**FIGURE 9** Verification statistics for reconstruction using the 1856–1922 calibration interval (as in Fig. 6).

resolve the same pattern of variability. The verification statistics are similar to those shown in Fig. 5. We may also compare the reconstructed time series [Eq. (10) with one mode of variability retained; see also Section 4.3.6] formed by using each of the chosen calibration intervals (1856–1922 and 1923–90) over their respective verification periods (1923–90 and 1856–1922). The reconstructions correlate with $r = 0.76$ (1923–90) and $r = 0.84$ (1856–1922); over the pre-observational interval 1001–1855, correlation between the two reconstructions is $r = 0.76$. For 11-year running averages, the two reconstructions correlate with $r \approx 0.9$ over the interval 1856–1990 and the full-time interval 1001–1990. However, there appears to be a tradeoff in skill between the North Pacific and eastern equatorial Pacific regions depending on the calibration period (compare Figs. 5 and 6 to Figs. 8 and 9). This finding suggests some sensitivity of H to the calibration interval chosen, which can affect the skill level by about 0.1 correlation unit in regions where TrSSTa has verifiable skill.

### 4.3.5.4. Comparison with Benchmark and Noise Reconstructions

In addition to checking the sensitivity of the results to map stability, we can also compare TrSSTa to an instrumental data-based reconstruction and a re-

construction based on calibrated red noise. Both experiments employ synthetic proxy data. In the first experiment, we reconstruct the SST field using SST, precipitation, and Palmer Drought Severity Index (PDSI) data from locations nearby the tree-ring indicator sampling sites (benchmark). In the second experiment, we perform the reconstruction based on randomly generated time series with normal distribution, unit variance, and lag −1 autocorrelation statistics of the tree-ring indicators (noise). The verification results obtained for these two experiments, using 1923–90 as a calibration period and reconstructing one pattern, are shown in Figs. 10 and 11, respectively. These results may be compared to those already shown in Fig. 6.

The calibrated skill in these experiments (results not shown) has spatial structure similar to that of TrSSTa (Fig. 5). Not surprisingly, the benchmark experiment has higher calibrated skill than TrSSTa, especially along the coasts of the Americas, and there is very little loss of skill (<0.1 correlation unit) between calibration and verification periods (results not shown). More surprisingly, our procedure was content to calibrate the noise proxy data at skill levels very similar to those of TrSSTa (results not shown). The true skill of the experiments, however, becomes apparent in the comparisons with withheld observed SST (Figs. 10a and 11a). While TrSSTa seems to capture the larger scale, open ocean

FIGURE 10 Verification statistics for benchmark reconstruction using calibration for 1923–90 (as in Fig. 6).
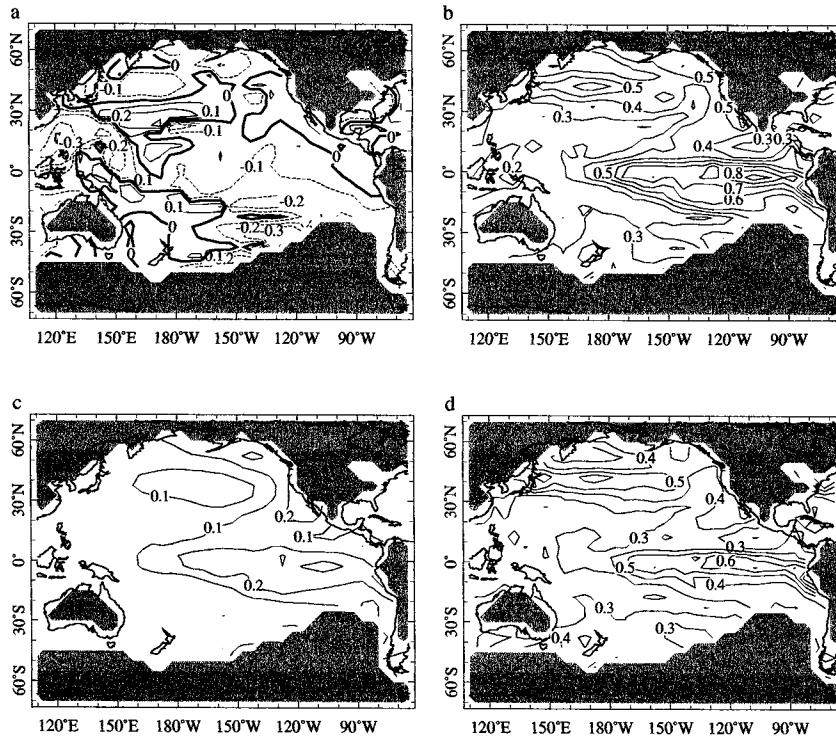
**FIGURE 11** Verification statistics for noise reconstruction using calibration for 1923–90 (as in Fig. 6).

signal and has less skill near the proxy sampling sites (Figs. 5–8), the benchmark experiment is more skillful in resolving smaller scale, coastal phenomena, with less skill in the subpolar North Pacific. We speculate that this may be due to temporal signal integration or other smoothing effects introduced by statistical development of the tree-ring chronologies, which may highlight the large-scale oceanographic signal. The noise experiment provides no verifiable skill, as expected (Fig. 11a). Due to the artificial calibrated skill, the reconstruction error is underestimated (Figs. 11b and 11d). However, since the noise reconstruction error (Fig. 11b) is only slightly larger than that of TrSSTa (Figs. 6b and 9b), the magnitudes of the respective reconstructed variances are similar (Figs. 6c, 9c, and 11c) and small relative to those of the benchmark experiment (Fig. 10c). These results suggest that TrSSTa has verifiable skill beyond that expected from red noise. However, the observational and mapping errors are large and must be correctly specified [Eq. (9)] to obtain reconstructions with amplitudes that are consistent with such errors. Verification exercises are required to clearly distinguish artificial skill from climatic information.

4.3.5.5. Rank of the Map H

We have shown results calibrating only the leading pattern of covariance between the SST and the tree-ring

indicators. This choice for the number of climatic patterns recoverable from this set of proxy data was motivated by PC and SVD analyses (Section 4.3.3, Fig. 3). Here, we examine the change in the results with increasing rank of $\mathbf{H}$ to see if additional patterns may be verifiably reconstructed. The calibration and verification skills for retention of two and three patterns are shown in Fig. 12. Over the calibration period 1923–90 (Figs. 12a and 12b), employing two or three patterns improves results marginally in the eastern equatorial Pacific and in the North Pacific. Verification results for the period 1856–1922 (Figs. 12c and 12d) show that skill is not increased by the additional patterns, although some redistribution of skill between the tropics and extratropics occurs. The changes in skill are similar in amplitude to those observed with reversed calibration and verification periods (Figs. 6 and 9). These observations are consistent with the choice of a rank 1 map for the CFR. Similarly, benchmark experiments retaining two and three patterns (results not shown) do not significantly improve on the verification statistics shown in Fig. 10. This result suggests that the number of patterns resolved in the present reconstruction is limited by the scarcity of proxy data employed as well as by the observational error. However, note also that while there is no increase in reconstruction skill with the rank of $\mathbf{H}$, there is little or no deterioration either, since additional modes contribute little variance to the reconstruction
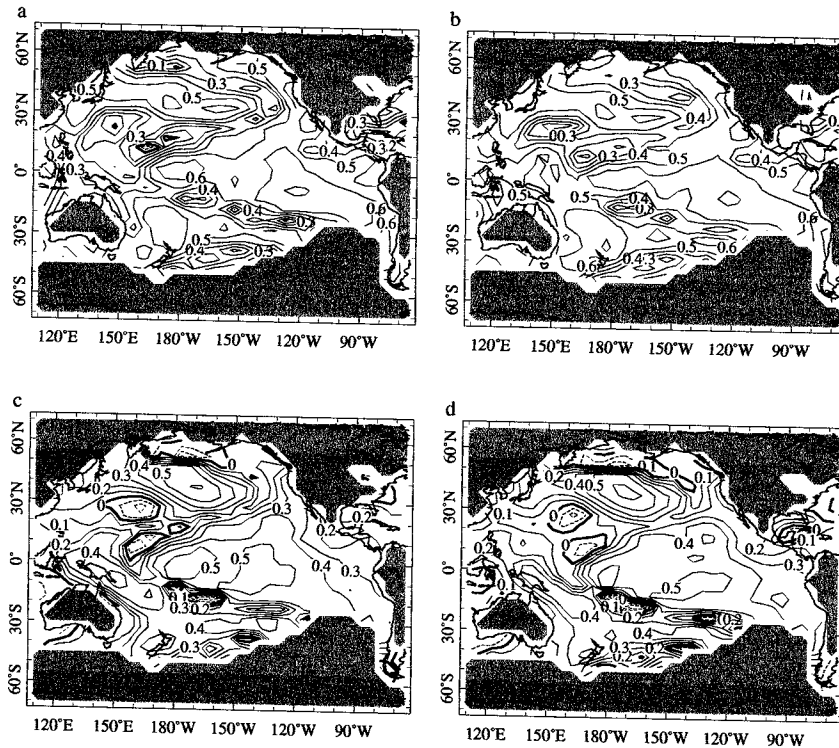
FIGURE 12   Calibration and verification correlation maps for reconstructions using 1923–90 calibration and two and three retained patterns (correlation units). (a) Calibration correlation (1923–90), two patterns retained. (b) Calibration correlation (1923–90), three patterns retained. (c) Verification correlation (1856–1922), two patterns retained. (d) Verification correlation (1856–1922), three patterns retained.

[Eq. (6); second term of Eq. (9)]. Hence, minimization of S makes the choice of the rank of **H** not as subjective as it might initially appear.

The preceding results suggest that while TrSSTa has skill over certain parts of the Pacific basin and in regions far removed from the tree-ring indicators, it does not have skill in all parts of the Pacific basin. In addition, as noted in Section 4.2 and shown here, variance resolved is a function of the quality of the map from climate record to proxy, as well as the proxy observational error. The first component is determined in the calibration stage of the procedure; the second component depends on the number of proxy indicators available for analysis as a function of time. In the most recent centuries of the reconstruction, all tree-ring indicators are available, and **H** is a full matrix. The analysis reconstructs anomalies with variance similar to that of the calibration period (e.g., Figs. 5c and 6c). However, as we proceed further back in time, fewer chronologies are available for analysis, and **H** becomes increasingly sparse. The observational error variance **R** grows (Section 4.3.4; Eq. (12)], and the analysis approaches zero or climatology, with the error almost the magnitude of the *true* or calibration period variance. However, since in this example most of the error in the reconstruction is

due to error in **H**, and since we resolve only a single pattern of climate variability, the reconstruction error remains large even into the relatively well-observed modern period. Additional proxy indicators sensitive to this leading mode of SST variability will be required to reduce the mapping error in the calibration stage, as well as to produce more accurate and precise reconstructions back through time.

4.3.6. Study of Climate Dynamics

4.3.6.1. Pacific Decadal SST Variability Inferred from Tree-Ring Indicators

Based on verification results (Figs. 5–8), we form an index from one of the most skillfully resolved regions, NINO3.4 (170°W–120°W, 5°S–5°N). Figure 13a shows the TrNINO3.4 SST anomaly; gray bars indicate 1σ error bars of this index. Since this reconstruction is composed of the time variation of a single mode of spatial variability, all such indices will be simple linear scalings of this time variation. We expect this index to be our best estimate of basin-scale SST variability, since the ratio of signal strength to analysis error is greatest in this region (Figs. 2 and 6). Correlation over the veri-
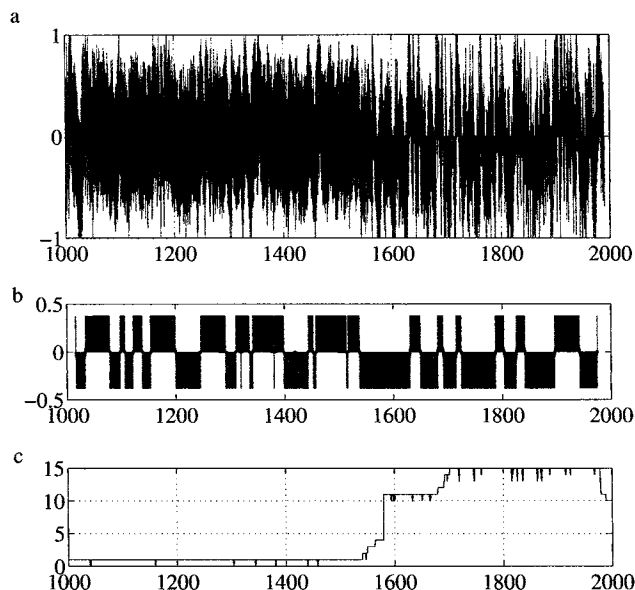
FIGURE 13 (a) NINO3.4 sea surface temperature (SST) anomaly (170°–120°W, 5°N–5°S) from tree-ring-based SST reconstruction (TrSSTa), A.D. 1001–1990. Units are degrees Celsius (°C). Shading indicates 1σ error estimates. (b) TrNINO3.4 index passed with a 31-year Gaussian filter. Overlain gray bars indicate the sign of the filtered index. Units are °C. (c) Number of tree-ring indicators available for analysis over this period.

fication period is 0.53. Figure 13b shows this index passed with a 31-year Gaussian filter. Overlain gray bars on this plot indicate whether the smoothed data show positive or negative anomalies.

Although in reality the NINO3.4 region is dominated by interannual variability, our verifiable reconstruction appears to be of ENSO-like, decadal variability (Figs. 2 and 13; Villalba et al., 2000). Note that the reconstruction prior to the 1590s is based upon only one time series (Fig. 13c), albeit one whose simultaneous contribution to the reconstruction is significant and stable in both calibration periods (Table 2). Given this caveat and the results of verification studies (Section 4.3.5), we interpret the results only qualitatively here. A shift to the positive phase of Pacific decadal variability occurs in the late 1970s. Other shifts occur ca. 1940 and 1895. Prior to 1895, TrNINO3.4 remains predominantly in the negative phase for several centuries, in rough correspondence to the Little Ice Age (LIA) interval noted from historical European climate data. Prior to the seventeenth century, decadal variability in this reconstructed mode was similar to that of the twentieth century; this suggests that twentieth-century Pacific decadal variability is not unprecedented. This result must be considered preliminary until more data can be brought into the analysis and the results are deemed stable to verification exercises.

4.4. CONCLUSIONS

The CFR described here has been derived by using a reduced space optimal estimation technique; the procedure is outlined in this chapter. Multiple benefits arise from placement of high-resolution paleoclimatological data within this context: (1) the solution is optimal (provided the a priori assumptions hold), (2) error estimates are provided for the solution, and (3) the solution and assumptions can be tested for mutual consistency.

As an application of this technique, we have reconstructed a single pattern of Pacific basin SST variability for the period A.D. 1001–1990, employing a set of Pacific American tree-ring indicators. The analysis produces SST field estimates with theoretical errors that are, at best, about twice the size of the historical SST analysis error of Kaplan et al. (1998) for the mid-nineteenth century and, at worst, as large as the RMS variance of modern observed SST. The results are encouraging enough to suggest that the tree-ring data from the Pacific coasts of North and South America may be used to reconstruct and study decadal- to century-scale SST variability. The results also demonstrate the nonlocal nature of the climatic information that may be extracted from this set of tree-ring data. However, benchmark and noise experiments show that verification tests are essential to determine the extent to which the reconstructions may be interpreted. Nevertheless, these reconstructions would benefit greatly from more spatially and temporally extensive proxy data sets, which should produce smaller errors in the reconstruction map and thereby more accurate results.

The results presented here are only a first application of the OA reconstruction method to proxy data (Fig. 1) and should be tuned and elaborated on in a number of ways. The algorithm for construction of the map from SST to tree-ring indicator may be designed to better incorporate frequency domain information likely to be well resolved by these particular proxy data (for example, after Mann and Park, 1994). Careful pretreatment of the tree-ring data, based on expert knowledge of the strengths and weaknesses of the tree-ring indicators, may be used to minimize known sources of bias and nonclimatic information. The resulting maps relating the climate field to the proxy variable will hopefully converge with theoretical or empirical studies of the links between proxy data and local climate and between local climate and large-scale climate variability. In turn, these improvements will result in better observational error covariance estimates, which are essential for proper use of the proxy data to form reconstruction estimates and to determine the true resolvable dimension of the map. Further improvements will exploit re-

solvable time transition information. Similar intercomparison studies between climate variables and other proxy data sources will provide similar characterizations of the information content of these data with respect to the large-scale climate field of interest. Similar work may also permit seasonal or single-season reconstructions. Subsequently, we may be able to merge the information provided by different proxy data sources to produce a reconstruction that takes no more or less than full advantage of each data source. Finally, a similar approach may be taken toward the reconstruction of other important climate fields such as air temperature and precipitation.

Acknowledgments

References

Bennett, A. F., 1992: *Inverse Methods in Physical Oceanography.* New York: Cambridge University Press.

Bottomley, M., C. K. Folland, J. Hsiung, R. E. Newell, and D. E. Parker, 1990: *Global Ocean Surface Temperature Atlas.* Norwich, England, U.K.: Her Majesty's Stationery Office.

Bradley, R. S., 1996: Are there optimum sites for global paleotemperature reconstruction? *In* Jones, P. D., R. Bradley, and J. Jouzel (eds.), *Climatic Variations and Forcing Mechanisms of the Last 2000 Years;* Vol. 41 of NATO ASI Series I: Global Environmental Change. New York: Springer-Verlag, pp. 603–624.

Bradley, R. S., and P. D. Jones, 1992: *Climate Since 1500 A.D.* London: Routledge.

Bretherton, C. S., C. Smith, and J. M. Wallace, 1992: An intercomparison of methods for finding coupled patterns in climate data. *Journal of Climate,* **5**: 541–560.

Briffa, K. R., and T. J. Osborn, 1999: Seeing the wood from the trees. *Science,* **284**: 926–927.

Cane, M. A., 1986: El Niño. *Annual Reviews of Earth and Planetary Sciences,* **14**: 43–70.

Cane, M. A., A. C. Clement, A. Kaplan, Y. Kushnir, R. Murtugudde, D. Pozdnyakov, R. Seager, and S.E. Zebiak, 1997: 20th century sea surface temperature trends. *Science,* **275**: 957–960.

Cane, M. A., A. Kaplan, R. N. Miller, B. Tang, E. C. Hackert, and A. J. Busalacchi, 1996: Mapping tropical Pacific sea level: Data assimilation via a reduced state space Kalman filter. *Journal of Geophysical Research,* **101**: 22599–22617.

Chang, P., L. Ji, and H. Li, 1997: A decadal climate variation in the tropical Atlantic Ocean from thermodynamic air-sea interactions. *Nature,* **385**: 516–518.

Clement, A. C., 1998: Mechanisms of tropical climate change: Glacial cycles to greenhouse warming. Ph.D. thesis. Columbia University, New York.

Clement, A. C., R. Seager, M. A. Cane, and S. E. Zebiak, 1996: An ocean dynamical thermostat. *Journal of Climate,* **9**: 2190–2196.

Cook, E. R., 1995: Temperature histories from tree rings and corals. *Climate Dynamics,* **11**: 211–222.

Cook, E. R., K. R. Briffa, and P. D. Jones, 1994: Spatial regression methods in dendroclimatology—A review and comparison of 2 techniques. *International Journal of Climatology,* **14**: 379–402.

Cook, E. R., B. M. Buckley, R. D. D'Arrigo, and M. J. Peterson, 2000: Warm-season temperatures since 1600 B.C. reconstructed from Tasmanian tree rings and their relationship to large-scale sea surface temperature anomalies. *Climate Dynamics,* **16**: 79–91.

Cook, E. R., D. M. Meko, D. W. Stahle, and M. K. Cleaveland, 1999: Drought reconstructions for the continental United States. *Journal of Climate,* **12**: 1145–1162.

Deser, C., M. A. Alexander, and M. Timlin, 1996: Upper-ocean thermal variations in the North Pacific during 1970–1991. *Journal of Climate,* **9**: 1840–1855.

Diaz, H. F., and N. E. Graham, 1996: Recent changes in tropical freezing heights and the role of sea surface temperature. *Nature,* **383**: 152–155.

Ebbesmeyer, C. C., D. R. Cayan, D. R. McLain, F. H. Nichols, D. H. Peterson, and K. T. Redmond, 1991: 1976 step in the Pacific climate: Forty environmental changes between 1968–1975 and 1977–1984. *In* Betancourt, J. L., and V. L. Tharp (eds.), *Proceedings of the Seventh Annual Pacific Climate PACLIM Workshop,* California Department of Water Resources, Interagency Ecological Studies Program Technical Report 26, pp. 115–126.

Enfield, D. B., and A. M. Mestas-Nuñez, 2000: Interannual to multidecadal climate variability and its relationship to global sea surface temperatures. *In* Markgraf, V. (ed.), *Interhemispheric Climate Linkages.* San Diego: Academic Press, Chapter 2.

Epstein, S., and C. J. Yapp, 1976: Climatic implications of the D/H ratio of hydrogen in C-H groups in tree cellulose. *Earth and Planetary Science Letters,* **30**: 252–261.

Evans, M. N., A. Kaplan, and M. A. Cane, 1998: Optimal sites for coral-based reconstruction of sea surface temperature. *Paleoceanography,* **13**: 502–516.

Evans, M. N., A. Kaplan, and M. A. Cane, 2000: Cross-validation of a sparse network of coral data and sea surface temperatures: Potential for coral-based SST field reconstructions. *Paleoceanography,* in press.

Evans, M. N., A. Kaplan, and M. A. Cane, 2000: Intercomparison of coral oxygen isotope data and historical sea surface temperature (SST): Potential for coral-based SST field reconstructions, *Paleoceanography,* **15**: 551–563.

Fritts, H. C., 1976: *Tree Rings and Climate.* New York: Academic Press.

Fritts, H. C., 1991: *Reconstructing Large-Scale Climatic Patterns from Tree-Ring Data: A Diagnostic Analysis.* Tucson: University of Arizona Press.

Fritts, H. C., T. R. Blasing, B. P. Hayden, and J. E. Kutzbach, 1971: Mulitvariate techniques for specifying tree-growth and climate relationships and for reconstructing anomalies in paleoclimate. *Journal of Applied Meteorology,* **10**: 845–864.

Gandin, L. S., 1965: *Objective Analysis of Meteorological Fields.* Jerusalem: Israeli Program for Scientific Translation, translated from the Russian, *Gidrometeorologicheskoye Izdatel'stvo,* Leningrad, Russia, 1963.

Hansen, J., and S. Lebedeff, 1988: Global surface air temperatures: Update through 1987. *Journal of Geophysical Research,* **92**: 13345–13372.

ITRDB, 1998: International Tree-Ring Data Bank. http://www.ngdc.noaa.gov/paleo/ftp-treering.html.

Jones, P. D., and K. R. Briffa, 1996: What can the instrumental record tell us about longer timescale paleoclimatic reconstructions? *In* Jones, P. D., R. Bradley, and J. Jouzel (eds.), *Climatic Variations and*

Forcing Mechanisms of the Last 2000 Years, Vol. 41 of NATO ASI Series I: Global Environmental Change. Berlin: Springer-Verlag, pp. 625–644.

Jones, P. D., R. S. Bradley, and J. Jouzel, 1996: *Climatic Variations and Forcing Mechanisms of the Last 2000 Years,* Vol. 41 of NATO ASI Series I: Global Environmental Change. Berlin: Springer-Verlag.

Jones, P. D., K. R. Briffa, T. P. Barnett, and S. F. B. Tett, 1998: High-resolution palaeoclimatic records for the last millennium: Interpretation, integration and comparison with General Circulation Model control run temperatures. *The Holocene,* 8: 455–471.

Kaplan, A., M. A. Cane, Y. Kushnir, A. C. Clement, M. B. Blumenthal, and B. Rajagopalan, 1998: Analyses of global sea surface temperature 1856–1991. *Journal of Geophysical Research,* 103: 18567–18589.

Kaplan, A., Y. Kushnir, and M. A. Cane, 2000: Reduced space optimal interpolation of historical marine sea level pressure: 1854–1992. *Journal of Climate,* 13: 2987–3002

Kaplan, A., Y. Kushnir, M. A. Cane, and M. B. Blumenthal, 1997: Reduced space optimal analysis for historical datasets: 136 years of Atlantic sea surface temperatures. *Journal of Geophysical Research,* 102: 27835–27860.

Krishna Kumar, K., R. Kleeman, M. Cane, and B. Rajagopalan, 1999: Epochal changes in the Indian monsoon-ENSO precursors. *Geophysical Research Letters,* 26: 75–78.

LaMarche, V. C., R. L. Holmes, P. W. Dunwiddie, and L. G. Drew, 1979: Chile. In *Tree-Ring Chronologies of the Southern Hemisphere,* Vol. 2 of Chronology Series V. Tucson: University of Arizona Press.

Latif, M., and T. P. Barnett, 1994: Causes of decadal climate variability over the North Pacific and North America. *Science,* 266: 634–637.

Lau, N. -C., and M. J. Nath, 1994: A modeling study of the relative roles of tropical and extratropical SST anomalies in the variability of the global atmosphere-ocean system. *Journal of Climate,* 7: 1184–1207.

Mann, M. E., and J. Park, 1994: Global-scale modes of surface temperature variability in interannual to century timescales. *Journal of Geophysical Research,* 99: 25819–25833.

Mann, M. E., R. S. Bradley, and M. K. Hughes, 1998: Global temperature patterns over the past five centuries: Implications for anthropogenic and natural forcing of climate. *Nature,* 392: 779–787.

Mann, M. E., R. S. Bradley, and M. K. Hughes, 2000: Long-term variability in the El Niño/Southern Oscillation and associated teleconnections. In Diaz, H. F., and V. Markgraf (eds.), *El Niño and the Southern Oscillation: Multiscale Variability and Global and Regional Impacts.* Cambridge, U.K.: Cambridge University Press.

Mardia, K. V., J. T. Kent, and J. M. Bibby, 1979: *Multivariate Analysis.* San Diego: Academic Press.

Martinson, D. G., K. Bryan, M. Ghil, M. M. Hall, T. R. Karl, E. S. Sarachik, S. Sorooshian, and L. Talley (eds.), 1995: *Natural Climate Variability on Decade-to-Century Time Scales.* Washington, DC: National Academy of Sciences.

Miller, R. N., 1990: Tropical data assimilation experiments with simulated data: The impact of the tropical ocean and global atmosphere thermal array for the ocean. *Journal of Geophysical Research,* 100: 13389–13425.

Namias, J., 1969: Seasonal interactions between the North Pacific Ocean and the atmosphere during the 1960s. *Monthly Weather Review,* 97: 173–192.

Namias, J., 1980: Causes of some extreme Northern Hemisphere cli-

matic anomalies from summer 1978 through the subsequent winter. *Monthly Weather Review,* 108: 1334–1346.

Parker, D. E., P. D. Jones, C. K. Folland, and A. Bevan, 1994: Interdecadal changes of surface temperature since the late nineteenth century. *Journal of Geophysical Research,* 99: 14373–14399.

Parthasarathy, B., K. R. Kumar, and A. A. Munot, 1991: Evidence of secular variations in Indian monsoon rainfall-circulation relationships. *Journal of Climate,* 4: 927–938.

Rao, C. R., 1973: *Linear Statistical Inference and Its Applications.* New York: John Wiley & Sons.

Ropelewski, C. F., and M. S. Halpert, 1987: Global and regional scale precipitation patterns associated with the El Niño/Southern Oscillation. *Monthly Weather Review,* 114: 2352–2362.

Smith, T. M., R. W. Reynolds, R. E. Livezey, and D. C. Stokes, 1996: Reconstruction of historical sea surface temperatures using empirical orthogonal functions. *Journal of Climate,* 9: 1403–1420.

Sokal, R. R., and F. J. Rohlf, 1995: *Biometry: The Principles and Practice of Statistics in Biological Research,* 3rd ed., New York: W. H. Freeman.

Stahle, D. W., R. D. D'Arrigo, P. J. Krusic, M. K. Cleaveland, E. R. Cook, R. J. Allan, J. E. Cole, R. B. Dunbar, M. D. Therrell, D. A. Gay, M. D. Moore, M. A. Stokes, B. T. Burns, J. Villanueva-Diaz, and L. G. Thompson, 1998: Experimental dendroclimatic reconstruction of the Southern Oscillation. *American Meteorological Society Bulletin,* 79: 2137–2152.

Trenberth, K. E., and T. Hoar, 1996: The 1990–1995 El Niño Southern Oscillation event: Longest on record. *Geophysical Research Letters,* 23: 57–60.

Trenberth, K. E., and J. W. Hurrell, 1994: Decadal atmosphere-ocean variations in the Pacific. *Climate Dynamics,* 9: 303–319.

Trenberth, K. E., and D. J. Shea, 1987: On the evolution of the Southern Oscillation. *Monthly Weather Review,* 115: 3078–3096.

Villalba, R., J. A. Boninsegna, T. T. Veblen, A. Schmelter, and S. Rubulis, 1997: Recent trends in tree-ring records from high elevation sites in the Andes of northern Patagonia. *Climatic Change,* 36: 425–454.

Villalba, R., R. D. D'Arrigo, E. R. Cook, G. Wiles, and G. C. Jacoby, 2000: Decadal-scale climatic variability along the extratropical western coast of the Americas: Evidence from tree-ring records. In Markgraf, V. (ed.), *Interhemispheric Climate Linkages.* San Diego: Academic Press, Chapter 10.

Wallace, J. M., 1996a: Observed climatic variability: Spatial structure. In *Decadal Climate Variability: Dynamics and Predictability,* Vol. 44 of NATO ASI Series I: Global Environmental Change. Berlin: Springer-Verlag, pp. 31–81.

Wallace, J. M., 1996b: Observed climatic variability: Time dependence. In Anderson, D. L. T., and J. Willebrand (eds.), *Decadal Climate Variability: Dynamics and Predictability,* Vol. 44 of *NATO ASI Series I: Global Environmental Change.* Berlin: Springer-Verlag, pp. 1–30.

Webster, P. J., 1994: The role of hydrological processes in ocean-atmosphere interactions. *Reviews of Geophysics,* 32: 427–476.

Wiles, G. C., R. D. D'Arrigo, and G. C. Jacoby, 1998: Gulf of Alaska atmosphere-ocean variability over recent centuries inferred from coastal tree-ring records. *Climatic Change,* 38: 289–306.

Wunsch, C., 1996: *The Ocean Circulation Inverse Problem.* New York: Academic Press.
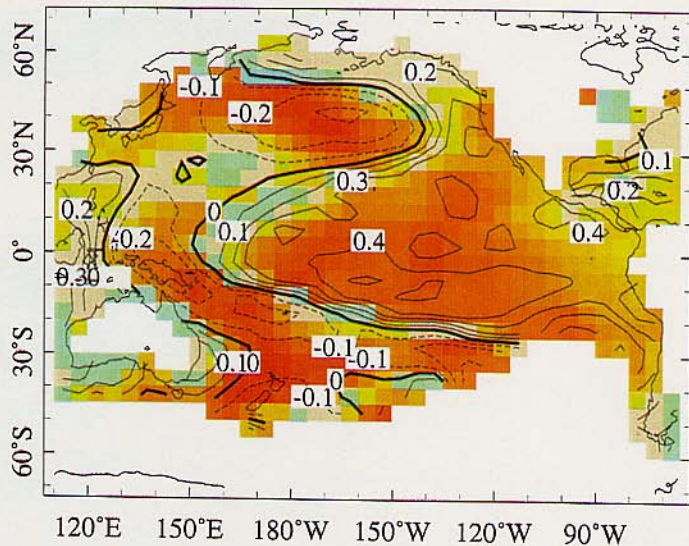
CHAPTER 4, FIGURE 7 Color plot of the verification correlation (Figure 6a) overlain by a contour plot of the correlation with the leading PC of the instrumental data from the tree-ring location (Figure 4b).